ROLE OF ORGANIC HYDROCARBONS IN ATMOSPHERIC ICE FORMATION VIA CONTACT FREEZING

A Thesis

by

KRISTEN NICOLE COLLIER

Submitted to the Office of Graduate and Professional Studies of
Texas A&M University
in partial fulfillment of the requirements for the degree of

MASTER OF SCIENCE

Chair of Committee,	Sarah Brooks
Committee Members,	Renyi Zhang
	Shari Yvon-Lewis
Head of Department,	Ping Yang

August 2016

Major Subject: Atmospheric Sciences

ABSTRACT

An optical ice microscope apparatus equipped with a sealed cooling stage and CCD camera was used to examine contact freezing events between a water droplet and ice nucleating particles (INP) containing either fresh or oxidized organic hydrocarbons. Samples were characterized using Fourier Transfer Infrared Spectroscopy and Raman Microspectroscopy. The organic hydrocarbons considered were octacosane, squalane, and squalene. All of the samples proved to be moderately efficient ice nuclei that induced freezing between -23 to -26 °C regardless of whether the INP was solid or liquid. Oxidation was shown to affect each INP differently, unlike what is seen in previous group results (Fornea et al., 2009; Brooks et al., 2014). Additionally, phase differences between compounds appear to correspond to whether oxidation improves ice nucleation efficiency. Oxidation of solid samples from previous work and new results indicate an improvement in ice nucleation efficiency by 1 to 2 °C. Ice nucleation results for liquid samples suggest varied effects on ice nucleation efficiency with oxidation depending on molecular process. Changes in sample viscosity as a result of oxidation of liquids appear to affect the ice nucleation ability. Exposure of liquid INP to oxidation resulted in an increase in viscosity for squalene and a decrease for squalane. A decrease in viscosity after oxidation corresponds to a decrease in ice nucleation ability of 1 to 2 °C. An increase in viscosity after oxidation is associated with an increase in ice nucleation ability by about 2-3 °C. Our results suggest that liquids can act as ice nuclei,

plausibly due to a decrease in the energy barrier brought about by the flexible nature of the molecules.

ACKNOWLEDGEMENTS

I would like to thank my committee chair, Dr. Sarah Brooks, and my committee members, Dr. Renyi Zhang, and Dr. Shari Yvon-Lewis, for their guidance and support throughout the course of this research.

I would like to thank each and every one of my group members for all of their helpful ideas and assistance with this study. I thank the department of Atmospheric Sciences faculty and staff for contributing to my excellent experience at Texas A&M University. I am grateful for the support of the National Science Foundation for providing funding for this study. Additional thanks for Raman data collected by Dr. Amanda E. Henkes, Materials Characterization Facility, Texas A&M University/Texas A&M Engineering Experiment Station.

Enormous thanks also go to my friends and family for their constant love and support. A special thanks to Mike for never ceasing to believe in me. Finally, thanks to my mom, dad, and brother for their love and encouragement over the past 25 years. I would also like to thank God for instilling in me an insistent wonder about the world and desire to learn.

TABLE OF CONTENTS

Page

LIST OF FIGURES

Page

LIST OF TABLES

Page

1. INTRODUCTION

A major uncertainty in climate models involves the formation of ice clouds. Atmospheric ice crystals are significant scatterers of light; hence, they can greatly impact the Earth's radiative budget (DeMott et al., 2010; Yi et al., 2013). Atmospheric aerosols, defined as a solid or liquid particle suspended in the atmosphere (Seinfeld and Pandis, 2016), can help facilitate the formation of ice in the atmosphere by acting as an ice nucleating particle (INP).

Ice formation occurs through several different processes in the atmosphere. Homogeneous freezing occurs at temperatures below ~-36 °C (Brooks et al., 2014). Above this temperature, heterogeneous freezing occurs with the aid of an INP. There are multiple pathways to heterogeneous freezing, including: contact, immersion, deposition, and condensation freezing (Figure 1).

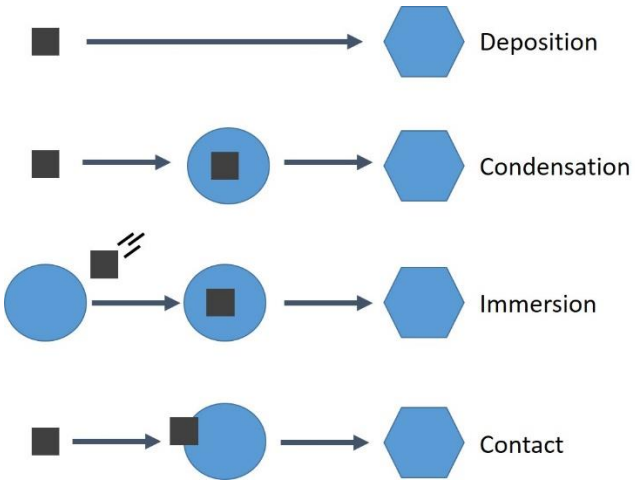

Figure 1: Heterogeneous mechanisms of ice nucleation.

The last of these, contact freezing, is the focus in this study. An ice nucleus acts to lower the energy barrier for the phase transition of water from liquid to solid. Contact freezing is a heterogeneous nucleation process in which contact between a supercooled liquid droplet and a particle cause the droplet to freeze. Traditionally, contact freezing was defined as the collision between a dry particle and a supercooled water droplet (Vali, 1985; Fletcher, 1969; Cooper, 1974). This was believed to generate a stable cluster of ice molecules that would act as a template to induce freezing of the whole droplet. More recent research suggests a different process leads to contact freezing (Fornea et al., 2009; Shaw et al., 2005). These studies propose that a lowering of the free energy barrier through contact, not the collision itself, is responsible for the initiation of freezing. As such, all freezing events in this study will be defined as surface contact between a droplet and an ice nucleus. Previous studies have indicated that contact freezing can cause droplets to freeze at warmer temperatures than other forms of

heterogeneous freezing (Fornea et al., 2009; Durant and Shaw, 2005; Shaw et al., 2005). It is hypothesized that certain characteristics in ice nucleating particles, such as surface chemistry and roughness of solid IN and viscosity of liquid IN, affect the IN's efficiency in this process. Characteristics of the ice nucleus, such as the chemical and physical properties, determine the temperature at which heterogeneous freezing will occur (Vali, 1985; Fornea et al., 2009). Identifying such properties is currently a major area of research.

In the atmosphere, INP may undergo certain aging processes such as oxidation. Determining the role various fresh and aged particles play in the formation of atmospheric ice crystals is crucial to improving climate and cloud microphysical models. For example, previous work studying the ice nucleating ability of fresh and oxidized soot has shown an improvement in ice nuclei efficiency with oxidative aging (Fornea et al., 2009). Oxidation is known to make an IN more hydrophilic, thus reducing the contact angle between the droplet and the surface (Fornea et al., 2009, Brooks et al., 2014).

Much previous work on ice nucleation ability has been performed on substances such as volcanic ash, soot, glucose, sucrose, and citric acid (Fornea et al., 2009; Baustian et al., 2013; Murray and Bertram, 2008; Murray, 2008). More research is needed on the effects of different structures of organic hydrocarbons on ice nucleation ability. Natural processes and human activities result in large amounts of organic compounds being emitted into the atmosphere (Val et al., 2011). These emissions sources include industrial activities, diesel fuel and biomass burning, as well as products from

incomplete combustion. Previous studies have reported these products as ranging in their ice nucleation ability (Brooks et al., 2014). Some are reported to be only moderately effective, meaning freezing is initiated just above the homogeneous freezing temperature (~-36 °C), while others have been shown to induce freezing at temperatures as warm as -15 °C (Brooks et al., 2014). There is uncertainty in the cause of this variability in ice nuclei efficiency for organic carbons. We postulate that the range of chemical and physical properties of these compounds reflect this wide range.

Aging, nanostructure, and porosity all have been shown to alter ice nucleation efficiency (Pöschl, 2011; Knopf et al., 2011; Kanji et al., 2013; Hiranuma et al., 2015; Chou et al., 2013; Brooks et al., 2014). Some studies suggest that a compound's structure influences the alignment of water molecules at the surface prior to freezing. When these molecules form a critical nucleus, defined as uniform alignment of a cluster of molecules within the water droplet, the droplet is observed to freeze (Lupi and Molinero, 2014). Other studies have cited a change in phase of particles that affects their ice nucleation ability (Wagner et al., 2012; Bogdan et al., 2014; Ignatius et al., 2015; Koop et al., 2011; Perraud et al., 2012, Debenedetti and Stillinger, 2001). Prior work has indicated that the aging process of oxidation alters the surface properties of a compound such that the ice nucleation efficiency is improved (Chughtai et al., 1991; Perraudin et al., 2007; Perraudin et al., 2007; Brooks et al., 2014). However, the way in which the particle surface is altered to induce this change is not known.

Recently, there have been several studies on the ability of amorphous solids to act as ice nuclei (Murray, 2008; Baustian et al., 2013; Dette and Koop, 2014; Cappa and

Wilson, 2011; Shiraiwa et al., 2011). Amorphous material are defined according to their viscosities, i.e. liquids ($<10^2$ Pa s), semi-solids ($\sim10^2$-10^{12} Pa s), and solids ($>10^{12}$ Pa s) (Koop et al, 2011). The last of these, with a viscosity greater than 10^{12} Pa s, are termed glassy solids. In glassy solids, molecules lack the high degree of alignment typically associated with a solid, but still maintain characteristics of the solid phase. Traditional ice nucleation theory suggests that the crystalline structure of solid particles act as a template for molecules in a water droplet to align into a crystalline pattern and form ice. Interestingly, several studies have revealed that semi-solids can act as effective INP (Wagner et al., 2012; Bogdan et al., 2014; Ignatius et al., 2015; Koop et al., 2011; Perraud et al., 2012, Debenedetti and Stillinger, 2001; Murray, 2008). It is likely that many secondary organic aerosols present in the atmosphere are amorphous (Virtanen et al. 2010). SOA have been observed to be effective INP (Knopf and Koop, 2006; Hoose and Möhler, 2012). Schill and Tolbert (2013) as well as Schill et al. (2014) report differences in the observed ice nucleation behavior of SOA, depending on whether the INP was a viscous liquid or a glass. In Murray (2008), citric acid is observed to readily nucleate ice and the viscosity of citric acid is examined for its role in ice nucleation. However, in that study, it was suggested that viscosity may inhibit ice formation due to inhibition of diffusion. This study aims to quantify the ice nucleating ability and viscosity of other organic aerosols to further define the role of viscosity in formation of ice in the atmosphere.

Modifications have been made to classical nucleation theory for heterogeneous freezing in order to obtain heterogeneous nucleation rate coefficients. One such model

combines the key elements of the stochastic process with the singular approach to ice nucleation. This computationally efficient model is known as the simplified Soccer Ball model (Niedermeier et al., 2014). The basis of this model is the idea that each IN contains a specific number of active sites and that nucleation at each of these sites will occur according to a specific nucleation rate coefficient (Niedermeier et al, 2011; Niedermeier et al., 2014). The nucleation rate coefficient is dependent on the contact angle of the critical cluster and the INP (Figure 2).

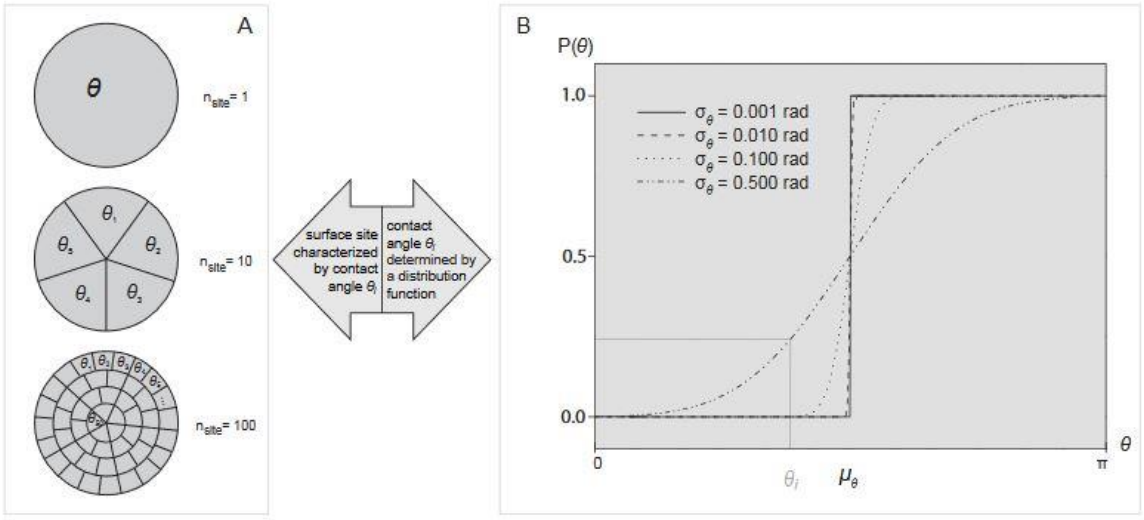

Figure 2: Visual of the concept of the simplified Soccer Ball model. Each particle surface is divided into a number of surface sites, n_{site}. Each n_{site} is characterized by contact angles with certain energy barriers. Adapted from: Niedermeier et al. (2011).

Using a range of contact angles on a single INP opposed to a single value has proven to provide a description of ice nucleation with better agreement with

experimental results (Welti et al., 2014; Luond et al., 2010). In this study, the simplified Soccer Ball model will be used to determine range in contact angle as a function of temperature as applied to our experimental results.

In the simplified Soccer Ball Model, it is assumed a population of particles is separated into n_{site} surface sites and a Guassian probability distribution function is used to find the contact angle, θ, in terms of the mean contact angle, μ_θ, and the standard deviation in contact angle, σ_θ (Zobrist et al., 2006):

$$p(\theta) = \frac{1}{\sqrt{2\pi}\sigma_\theta} \exp(-\frac{(\theta - \mu_\theta)^2}{2{\sigma_\theta}^2})$$

The probability of freezing in the simplified Soccer Ball model is identical for all particles since the particles are assumed to be homogeneous surfaces making $n_{site} = 1$. The probability of a single droplet not being frozen is

$$P_{unfr}(T, \mu_\theta, \sigma_\theta, t) = \int_0^\pi p(\theta) \exp(-j_{het}(T, \theta) s_{site} t)\, d\theta + \int_{-\infty}^0 p(\theta) \exp(-j_{het}(T, \theta = 0) s_{site} t)\, d\theta + \int_\pi^\infty p(\theta) \exp(-j_{het}(T, \theta = \pi) s_{site} t)\, d\theta$$

where T is temperature, s_{site} is the surface area of a nucleation site, and t is time. j_{het} is the nucleation rate coefficient and is defined as

$$j_{het}(T) = \frac{kT}{h} \exp(-\frac{\Delta F_{diff}(T)}{kT}) \left[n \exp(-\frac{\Delta G(T) f}{kT}) \right]$$

where ΔF_{diff} represents the activation energy of water molecules diffusing across a solid-liquid interface, ΔG is the Gibbs free energy of formation for a critical cluster, n is the number density of water molecules at the ice/water interface, f is the wetting parameter, k is the Boltzmann constant, and h is Planck's constant. Values for each of these constants were provided by Zobrist et al. (2007), with the exception of wetting parameter, f. The wetting parameter is a function of contact angle, θ, and described below.

$$f = \frac{1}{4}(2 + cos\theta)(1 - cos\theta)^2$$

Next, the fraction frozen for a droplet population interacting with IN of various type at a given temperature is

$$P_{fr}(T, \mu_\theta, \sigma_\theta, t) = 1 - P_{unfr}(T, \mu_\theta, \sigma_\theta, t)$$

An underlying assumption of the model is that a reduction in contact angle correlates with an increase in hydrophilicity, which yields a more effective IN (Pruppacher and Klett, 2000).

Some organic hydrocarbons which are present in the atmosphere and may act as INP are compounds that represent organic hydrocarbons from diesel motor oil and other fuel blends, including octacosane, squalane, and squalene (Table 1). Octacosane is a straight chain saturated alkane ($C_{28}H_{58}$) in solid crystalline form. Both squalane and squalene are liquids with squalane being a highly branched saturated alkane ($C_{30}H_{62}$), and squalene a branched unsaturated alkene ($C_{30}H_{50}$).

Table 1: List of organic hydrocarbons used in this study.

Name	Structure	Chemical Formula	Molecular Mass (g/mol)	Purity (%)
Octacosane	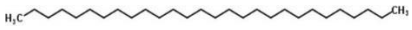	$C_{28}H_{58}$	394.76	99
Squalane	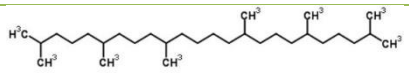	$C_{30}H_{62}$	422.81	99
Squalene	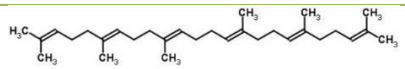	$C_{30}H_{50}$	410.72	98

All samples are supplied from Sigma Aldrich.

Squalane and squalene are of particular interest since, to the best of our knowledge, true liquids have not been previously tested as ice nuclei. There is potential for the liquid to mix with the water droplet or become glassy as the temperature decreases. It is the intent of this study to contribute to this understanding. Although the ability of many compounds to act as INP are now well characterized (DeMott, 1995; Kanji and Abbatt, 2006; Durant et al., 2006; Knopf and Koop, 2006; Möhler et al., 2006, Shaw et al., 2005), more measurements are needed for organic hydrocarbons and their aged counterparts. This study will be used to elucidate the role of these organic hydrocarbons (fresh and oxidized) as INP via contact freezing. In addition, we will evaluate the role of viscosity in ice nucleation.

2. EXPERIMENTAL METHODS

2.1 Sample Preparation

A custom ice microscope apparatus was used to obtain a series of single droplet-single ice nuclei heterogeneous freezing temperatures, as used in our previous studies (Brooks et al., 2014; Fornea et al., 2009). Approximately 0.0005 g of material were used for solid compounds, and 2 μL were used for liquid compounds. These amounts are in line with our previous work completed (Brooks et al., 2014; Fornea et al., 2009). While the sample dimensions employed here are significantly larger than atmospheric aerosol systems, the apparatus design makes it possible to determine the temperature of freezing via both immersion and surface-initiated contact freezing (Fornea et al., 2009). The compounds used as representative ice nuclei for this study are organic hydrocarbon compounds, including octacosane, squalane, and squalene. The same method as our previous work was employed for the solid samples. The octacosane experiments in this study were conducted in contact mode, by positioning a 0.0005 g octacosane particle in direct contact with a 2 μL liquid water droplet. The same process could not be replicated with squalane and squalene, however, because they are both liquids. In this case, a micropipette was used to position a 2 μL drop of the sample in contact with a 2 μL water droplet.

Commercially available octacosane (Alfa Aesar, 99% purity), squalane (Alfa Aesar, 98% purity), and squalene (Alfa Aesar, 98% purity) were used in this study.

Fresh samples were obtained directly from the commercial bottle in 1 g or 2 mL amounts for solids and liquids, respectively. To oxidize a solid sample (Figure 3), 10 g of material were placed on a glass fiber filter (Adventec) inside of a Nalgene chamber. A HC-30 generator (Ozone Solutions) was used to produce ozone for the oxidation process. A mass flow controller (Model MC-10 SLPM-D, Alicat) controlled a 0.01 L/minute flow of oxygen into the generator. Within the generator, the oxygen passes through a corona cell which causes a fraction of the molecular oxygen to divide into atomic oxygen. Next, the atomic oxygen reacts with the remaining diatomic oxygen to form high concentrations of ozone (5-14% by weight or 50,000-140,000 ppm). Following this, the ozone is diluted with nitrogen to yield an ozone concentration near 80 ppm, which enter the Nalgene chamber. A UV absorption analyzer (UV-100, Eco Sensors, Inc., 254 nm), is used to continuously monitor ozone concentration throughout the oxidation process. After a 24-hour exposure period, the sample was removed and stored in an amber jar to prevent further oxidation.

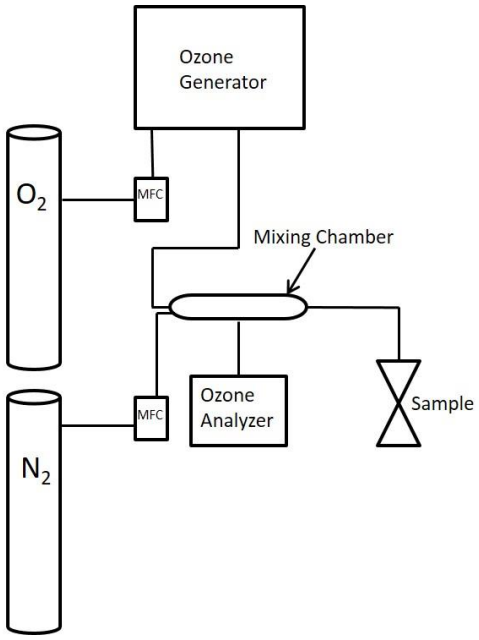

Figure 3: Schematic of the oxidation setup. The object labeled sample represents the Nalgene chamber or impinger, depending on whether a solid or liquid sample is being oxidized, respectively.

To oxidize liquid samples, 10 mL of organic compound (i.e. squalane or squalene) were placed inside a glass impinger instead of the Nalgene chamber. This allows ozone to bubble through the sample to oxidize it. As with the solid sample, the ozone was introduced into the sample at a concentration of about 80 ppm. The UV absorption analyzer was used to monitor the ozone concentration throughout the 24-hour exposure period. When the oxidation process was complete, the oxidized samples were transferred to amber jars for storage to prevent further oxidation.

2.2 The Ice Microscope

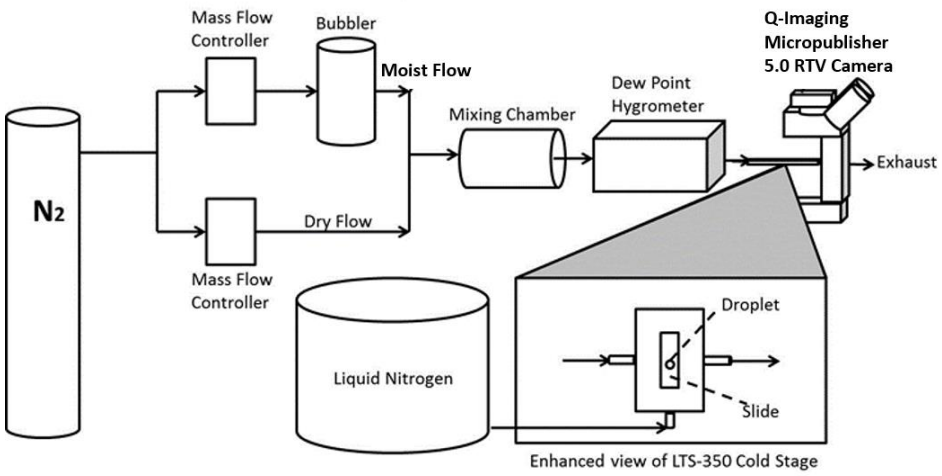

Figure 4: Ice microscope apparatus (modified from Fornea et al., 2009).

The procedure for completing a contact freezing experiment for a solid sample are described in detail in Fornea et al., 2009, and is thus briefly described here. The ice microscope apparatus includes an Olympus optical microscope (model BX51M), a digital camera (Q-Imaging Micropublisher 5.0 RTV), and a sealable Linkham cooling stage (Figure 4). The cooling stage allows temperature control to within ± 0.1 °C. With this setup, multiple independent freezing temperature measurements can be performed with a single droplet-IN system.

Experiments began by using an Ependorf micropipette to position a 2 μL droplet of ultrapure water (Aqua Solutions, HPLC grade) on a pre-cleaned slide that had been

subjected to a 1.0% AquaSil solution (Pierce Chemical Company) coating to create a hydrophobic surface. For solid samples, the tip of a pipette was used to position the sample in contact with the droplet. For liquid samples, the micropipette was used to place 2 μL of the sample in contact with the water droplet.

Once the sample and droplet are in place on the slide, the stage was sealed and cooled at 1.0 °C/min from 5 °C down to -40 °C. This temperature range has been chosen to represent the span in which a droplet is expected to freeze without the aid of a particle. A camera mounted on top of the microscope (Figure 4) captures an image every 6 seconds which corresponds to 1 image every 0.1 °C temperature change. A low humidified nitrogen flow is introduced into the sealed stage to prevent droplet evaporation throughout the experimental runs. This flow is generated through the mixing of dry nitrogen (0.6 lpm) with that of nitrogen that has become saturated from flowing through a bubbler (0.01 lpm). A hygrometer (EdgeTech DewPrime II, Model 2000) is used to monitor the relative humidity of the moist flow. The relative humidity is maintained at approximately 0% to prevent droplet evaporation, but ensure that condensation does not form inside the sealed cooling stage. Once the cooling stage reaches a temperature of -40 °C, it next is warmed to 5 °C at 1.0 °C/min. The temperature is maintained at 5 °C for one minute to ensure that the droplet has completely melted before the next cooling cycle begins. Although each cycle within an experiment is performed with a single droplet-IN setup, all individual experiments require a fresh droplet-IN to be used. Once the experiment is complete, the images may be viewed to determine freezing onset temperatures on a frame-by-frame basis. A

freezing event is distinguished by a change in opacity of the droplet (transparent to opaque) between frames, as seen in Figures 5 and 6.

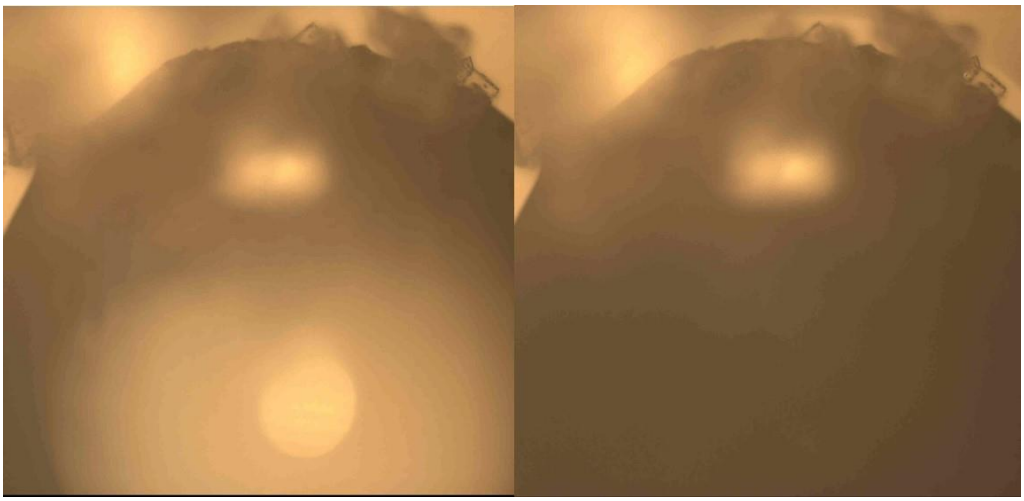

Figure 5: An example of a freezing event using a solid sample in contact with a water droplet. These are two consecutive images captured by the CCD camera.

Figure 6: An example of a freezing event between a liquid sample in contact with the water droplet. These are two consecutive images captured by the CCD camera.

The two previous figures illustrate freezing events as identified using consecutive images captured by the CCD camera. Figure 5 shows a solid aerosol in contact with the water droplet. The droplet becomes opaque when it freezes, so the freezing event may be identified. Figure 6 is very similar, but this time illustrates the change in opacity that occurs for a water droplet when it freezes in contact with a liquid sample. The liquid sample is surrounding the droplet.

Each experiment produces approximately 20 independent freezing data points. There is slight variation in the number of data points collected for each run due to consumption of the liquid nitrogen supply prior to the end of the series.

2.3 Sample Characterization

2.3.1 Fourier Transfer Infrared Spectroscopy (FTIR-HATR)

Fourier transfer infrared spectroscopy with horizontal attenuated total reflectance (FTIR-HATR) was used to characterize changes in chemical composition. This method of sample characterization is in line with previous work on soot and polycyclic aromatic hydrocarbons (Brooks et al., 2014). The FTIR-HATR is a PerkinElmer Spectrum 100. Samples are placed on a zinc selenium crystal and inserted into a sealable HATR chamber (Pike Technologies) for analysis. The solid samples are mixed with reagent grade acetone before being put on the crystal. Once the acetone evaporates (~30 minutes), a uniform layer of the organic hydrocarbon remains on the crystal. Liquid samples are placed directly onto the crystal since they already form a uniform layer. A wavenumber range of 4000-700 cm^{-1} is used to measure absorbance with a resolution of 2 cm^{-1}. All fresh and oxidized samples were analyzed using these methods (Brooks et al., 2014). The spectra for the fresh samples were subtracted from their respective oxidized spectra to obtain a difference spectrum. The difference spectra is used to confirm that oxidation occurred as well as indicate other changes in the chemistry of the compounds.

2.3.2 Raman Microspectroscopy

Raman microspectroscopy was also used to characterize changes in the chemical composition of the samples as a result of oxidation. This method was used in addition to the FTIR-HATR characterization in order to characterize how the surface and bulk of the samples changed due to oxidation. A similar method was utilized in previous work to characterize sample aging (Avzianova and Brooks, 2013; Deng et al., 2014; Avzianova and Brooks, 2014). It is theorized that oxidation of a solid sample will occurs at the surface of the particle due to slow internal mixing. Therefore, a more noticeable oxidation will be seen on the surface of the solid sample than in the bulk. Conversely, the high degree of internal mixing associated with liquids will lead to a more uniform oxidation throughout the sample. The Raman is a Horiba Jobin Yvon LabRam HR Raman microscope with a 633 nm laser. Raman characterization was carried out at the Texas A&M Materials Facility. Solid samples were analyzed using a 50x SLM objective using a large pinhole and a small pinhole to examine differences between surface sample and bulk. The larger pinhole was 200 microns and used to analyze the bulk of the solid sample. The smaller pinhole was 50 microns and was used to observe the surface of the sample. Liquid samples were examined using a 4x cuvette holder and a 50x SLM objective under the microscope.

2.4 Viscosity

A significant phase change was observed when squalene was oxidized. Qualitatively, the squalene became very thick and highly viscous upon oxidation. This phase change posed an interesting question about whether viscosity plays a role in IN

ability. After FTIR-HATR and Raman characterization, the liquid samples were measured for viscosity. A viscometer was used to determine the viscosity of the liquid samples, and the effects of temperature and oxidation on sample viscosity. A glass capillary viscometer (Ubbelohde Viscometer Cannon Instruments Co., size 3B, Cole-Parmer) was filled with sample and submerged into a Neslab tank (Neslab ULT 80/95, Thermo Electron Corporation) that is held at a constant temperature. Representative temperatures within the range of the ice microscope were chosen to obtain a profile of viscosity change with temperature: 10°C, 5°C, -10°C, -20°C, -30°C, and -40°C. The viscometer remained in the bath for 20 minutes at each temperature set point to equilibrate to a uniform temperature before measurements were taken. Then, suction was used to draw the sample up the viscometer and a timer was used determined the amount of time it took the bottom of the sample meniscus to move from point A to point B within the viscometer (Figure 7).

Figure 7: Ubbelohde Viscometer Cannon Instruments Co., size 3B. The capillary viscometer is used to measure viscosity of liquid samples by measuring the time the sample takes to move from point A to point B.

Viscosity is measured by filling the viscometer with the liquid sample and drawing it up through suction to the chamber above point A. Next, a timer is used to

measure how long it takes, in seconds, for the sample to fall from point A to point B. Then, the formula below, is used to calculate the viscosity of the sample.

This process was repeated for each temperature point for fresh and oxidized squalane and squalene. Three tests were taken at each temperature and the average viscosity plotted to indicate the samples change with temperature. The viscosity is determined using the following formula:

$$\eta = t * c * \rho,$$

where η is viscosity, t is time (s), c is the viscometer constant, and ρ is the density (g/mL).

3. RESULTS

3.1 Cold Stage Calibration

A three point calibration of the cold stage was performed to verify accuracy (Figure 7). Three compounds were chosen for the calibration based on their well-documented freezing temperatures that are representative of the temperature range used. These compounds are n-dodecane, n-undecane, and n-decane (Sigma Aldrich).

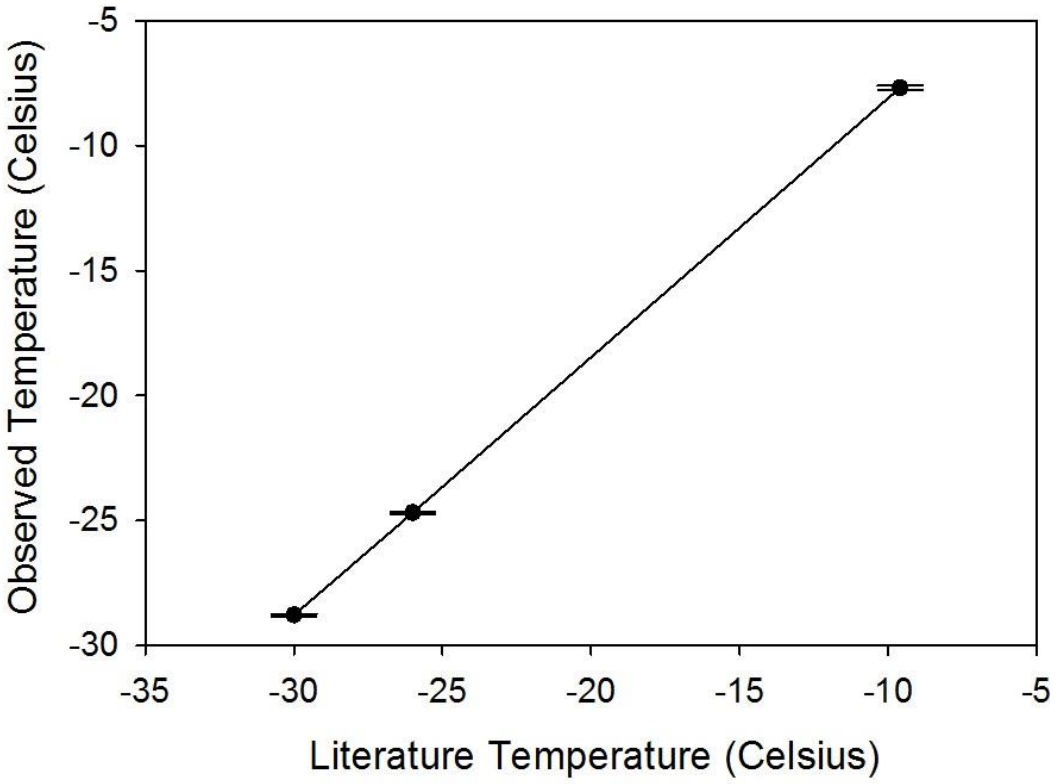

Figure 8: Three point calibration of the cold stage. Experimental temperature values are plotted against values collected from the literature (Sigma Aldrich). The trendline was calculated to be y = 1.04x + 2.25.

Table 2 summarizes the calibration. Each sample was averaged for three separate experimental runs and the pooled standard deviation was calculated.

Table 2: Summary of the three point calibration performed on the cold stage.

Compound	Literature Value	Observed Value	Pooled Standard Deviation in Observed Value
Dodecane	-9.6	-7.68	0.09
Undecane	-26.0	-24.69	0.05
Decane	-30.0	-28.78	0.05

A trendline was calculated from plotting the data (Figure 8). The trendline equation is y = 1.0351x + 2.2519. This indicates the cold stage is off by about +2 degrees. The equation was used to apply a correction to all of the data collected, to account for this difference in temperature recorded by the cold stage. The observed temperature was used as the y value in the equation and the resulting x-value that was calculated gave the corrected form of the data.

3.2 Fresh and Oxidized Organic Hydrocarbons as Ice Nuclei

Freezing discrepancies between fresh and oxidized organic hydrocarbons can easily be summarized by graphing the full data set for each different sample. Figures 8, 9, and 10 depict the differences between fresh and oxidized samples octacosane, squalane, and squalene, respectively. Each line represents one experimental run. Each experimental run consists of one particle and one water droplet that are cycled through the temperature cycle. There is variation in the number of cycles due to the liquid nitrogen running out at different points in the experimental runs. Fresh samples are

indicated by lines with black circle markers. Oxidized samples have been identified by a white diamond marker.

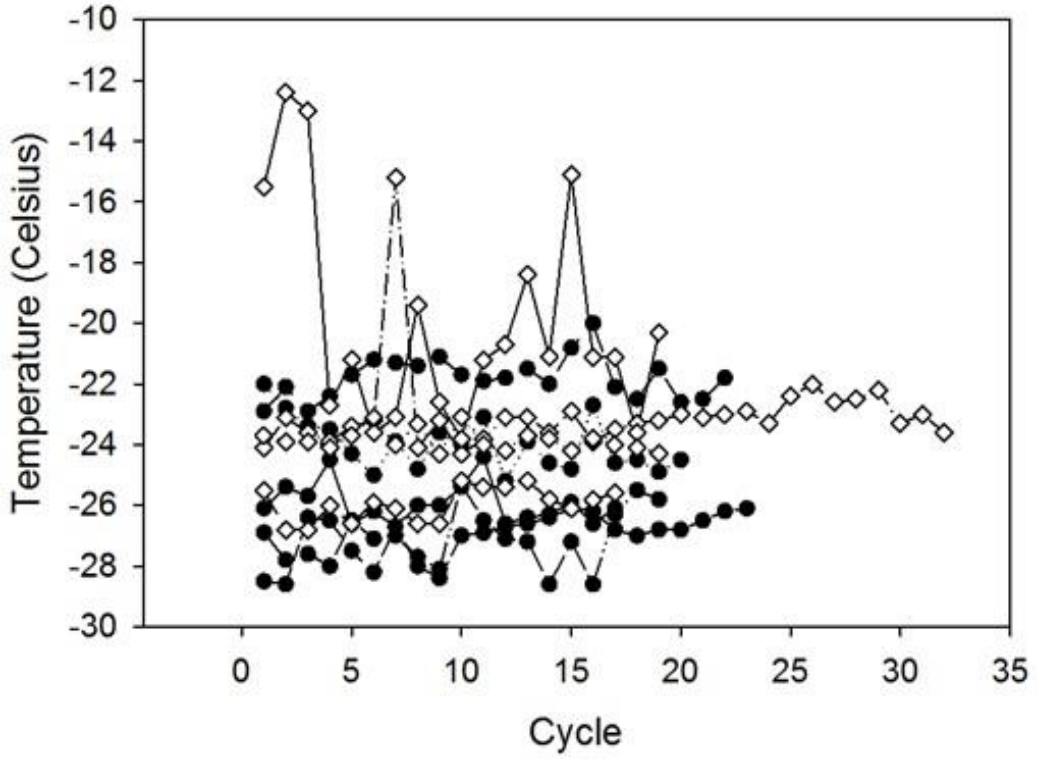

Figure 9: Freezing temperatures for 275 micron diameter fresh (black circles) and oxidized octacosane (white diamonds). Each line represents a series of experiments conducted with a single particle as an ice nucleus.

Of all of the samples tested, the octacosane showed the most variability throughout each experimental run. A possible reason for this is changes in the surface features of the solid octacosane sample upon successive heating and cooling cycles. The liquid samples show much more consistency throughout the experimental runs.

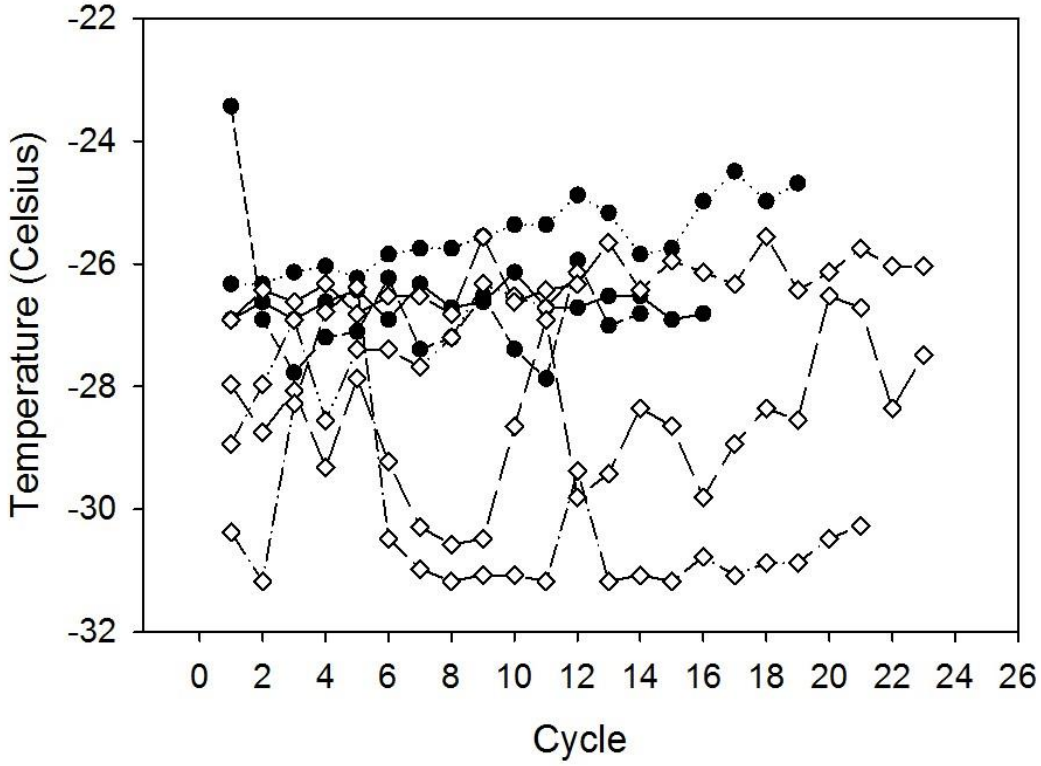

Figure 10: Freezing temperatures observed for fresh (black circles) and oxidized (white diamonds) squalane in contact with a water droplet.

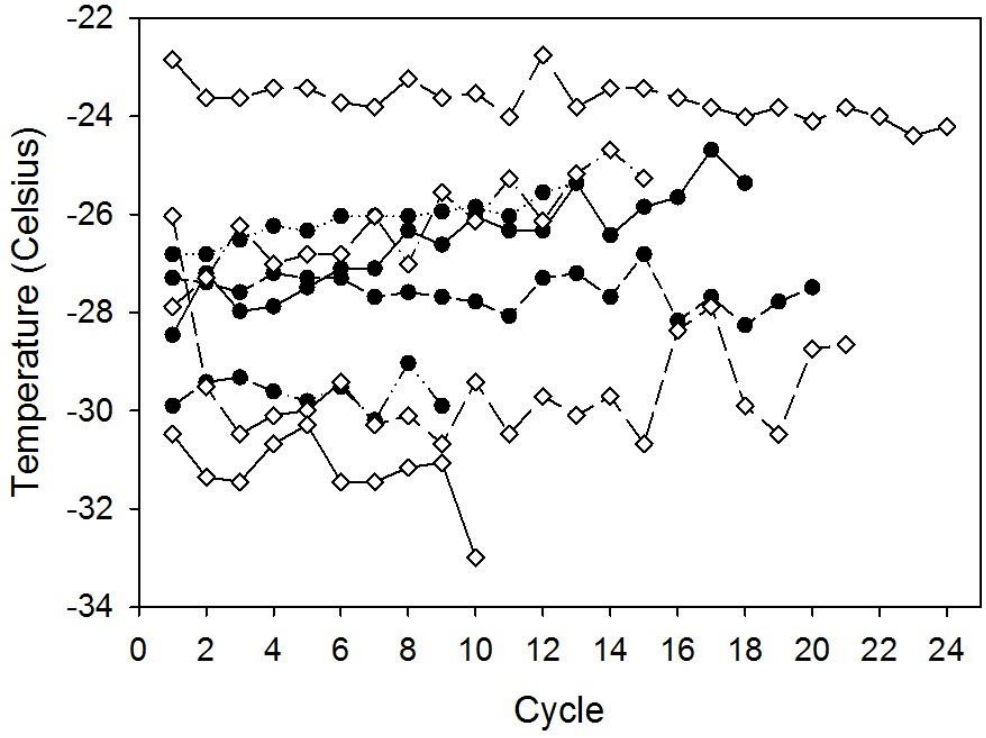

Figure 11: Observed contact freezing temperatures for fresh (black circles) and oxidized (white diamonds) squalene samples.

Based on the results of Figures 9-11, it appears that all of these organic hydrocarbons are moderately effective IN, that induce contact freezing, on average, around -25 °C. Table 3 summarizes the mean freezing temperature for each sample collected in this study.

Table 3: Mean freezing temperatures for fresh and oxidized samples. Uncertainty is reported as a pooled standard deviation.

IN Composition	Diameter (μm)	No. of Experiments	No. of Freezing Temperature Data Points	Mean Freezing Temperature (°C)
Fresh Octacosane	275	5	101	-25.19 ± 0.81
Oxidized Octacosane	275	4	87	-24.28 ± 1.1
Fresh Squalane	~781	4	58	-25.65 ± 0.68
Oxidized Squalane	~781	4	79	-26.67 ± 1.05
Fresh Squalene	~781	4	60	-25.97 ± 0.66
Oxidized Squalene	~781	5	91	-23.34 ± 0.92

Freezing is observed to occur near -25.6 on average for all fresh samples combined. Joined with previous work using soot and polycyclic aromatic hydrocarbons (Fornea et al., 2009; Brooks et al., 2014, Hiranuma et al., 2015), all organics appear to behave as moderate ice nuclei despite molecular structure differences.

3.3 Liquids as Ice Nucleating Particles

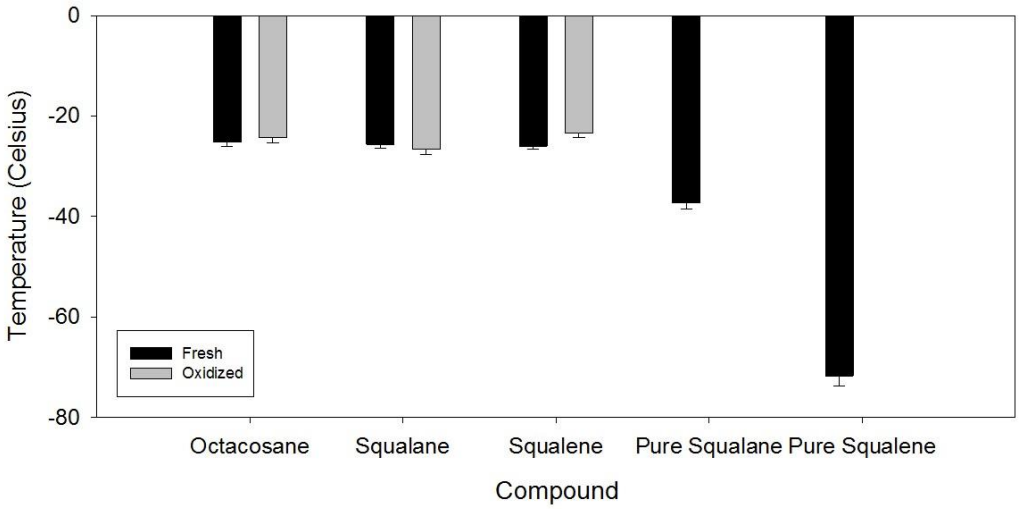

Figure 12: Contact freezing temperatures for fresh and oxidized organic hydrocarbon nuclei are compared to the freezing temperatures of pure liquid samples. The liquid samples freeze at temperatures below the temperature at which they initiate contact freezing.

Figure 12 presents the contact freezing temperatures of each organic hydrocarbon with a water droplet, and observed freezing temperatures of pure liquid samples, obtained from freezing experiments using the ice microscope apparatus. Contact freezing temperatures for oxidized samples are shown in conjunction with their fresh counterparts. Overall, the three organic hydrocarbons observed all act as moderately effective ice nuclei in both fresh and oxidized samples.

An interesting result of this study is the freezing of water droplets in contact with liquid aerosols. Several recent studies have examined the importance of glassy or

amorphous aerosols as ice nuclei (Ignatius et al., 2015; Wagner et al., 2012; Bogdan et al., 2014), but there are very few results on viscous liquids as ice nuclei. Several experiments were conducted to ensure that the liquid samples were in fact acting as ice nuclei in the contact freezing mode, opposed to other processes affecting initiation of ice formation such as freezing of the INP or mixing of the INP and water droplet.

Originally, we hypothesized that the liquid samples were mixing with the water droplet throughout the experimental run and initiating freezing after becoming a solution. To test this hypothesis, food coloring was added to the droplet and a contact freezing experiment was set up. The food colored droplet and sample were observed throughout the experiment for any indication of mixing. Images at the beginning of the experiment, upon freezing and melting of the droplet, and at the end of the experiment were all closely examined. This qualitative analysis indicated no mixing of the sample and the droplet throughout the experiment.

Another hypothesis was the possible freezing of the liquid drop prior to the freezing of the water droplet. If the sample were to freeze before contact freezing occurred, it would indicate the sample was initiating ice nucleation in its solid form. Analysis of this was completed by conducting a freezing experiment for each organic liquid sample in its pure form (i.e. without a water droplet), to determine at what point the sample froze. In our experiment, pure squalene was observed to freeze at -71.77 ± 2.05 °C, consistent with a literature value of -75 °C (Sigma Aldrich). This indicates the squalene remains in the liquid phase when contact freezing occurs. Pure squalane has a freezing temperature of -38 °C (Sigma Aldrich) and was observed to freeze at -37.33 ±

1.1 °C experimentally. In other words, the pure squalene remains in the liquid phase until well below the freezing temperature of water in contact with squalene droplets. This provides significant evidence of squalane and squalene are in the liquid phase when they facilitate contact freezing of a water droplet.

3.4 Exposure to Ozone

Oxidative aging by exposure to ozone is analyzed in this section. Both Raman microspectroscopy and FTIR-HATR spectroscopy were analyzed for fresh and oxidized samples to characterize the effects of oxidation on the sample and ensure that oxidation had occurred.

Figures 12, 13, and 14 depict the FTIR spectra for octacosane, squalane, and squalene, respectively. Each graph displays the spectrum for a fresh sample, an oxidized sample, and the difference between these two. The difference spectra are created by subtracting the fresh spectrum from the oxidized spectrum. A difference spectrum is useful in identifying changes in the features of the spectra as a result of oxidation. The three spectra on each graph are offset to make each line visible and easier to compare.

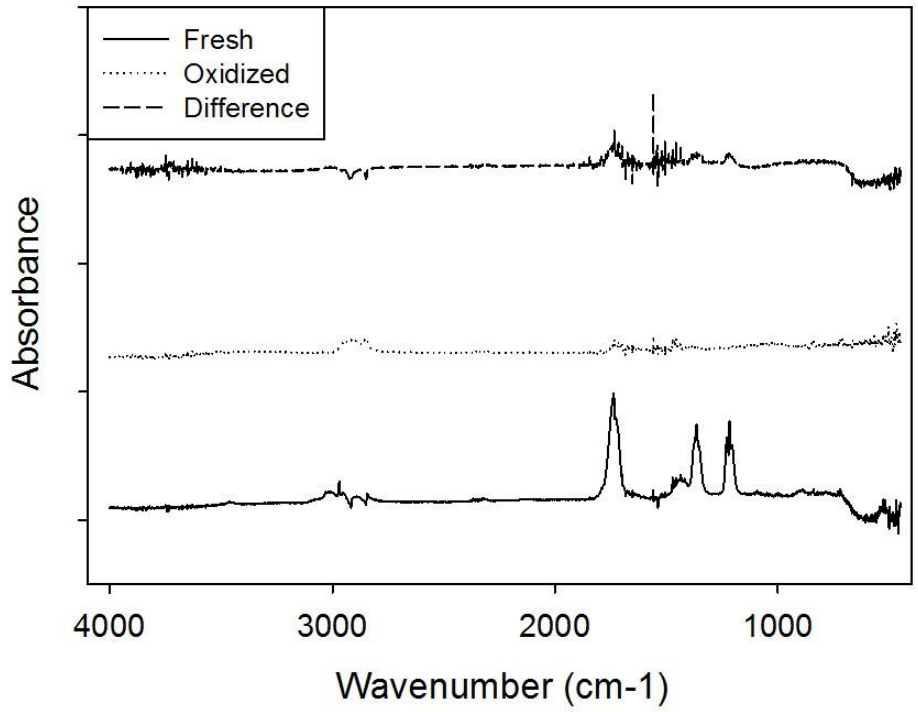

Figure 13: FTIR-HATR spectra for octacosane. Major peaks in the difference spectrum are identified and discussed further in the text.

The major peaks in the FTIR-HATR octacosane difference spectrum (Figure 13) centered around 2970 cm^{-1} and 1365 cm^{-1} are characteristic of C-H stretch and –C-H bends, respectively, found in alkanes. The peaks that indicate oxidative changes have occurred are located at 1735 cm^{-1} and 1215 cm^{-1}. The peak at 1735 cm^{-1} is a C=O stretch associated with a functional group of carbonyls or aldehydes. The peak at 1215 cm^{-1} is a C-O stretch that is representative of ethers, acids, and esters.

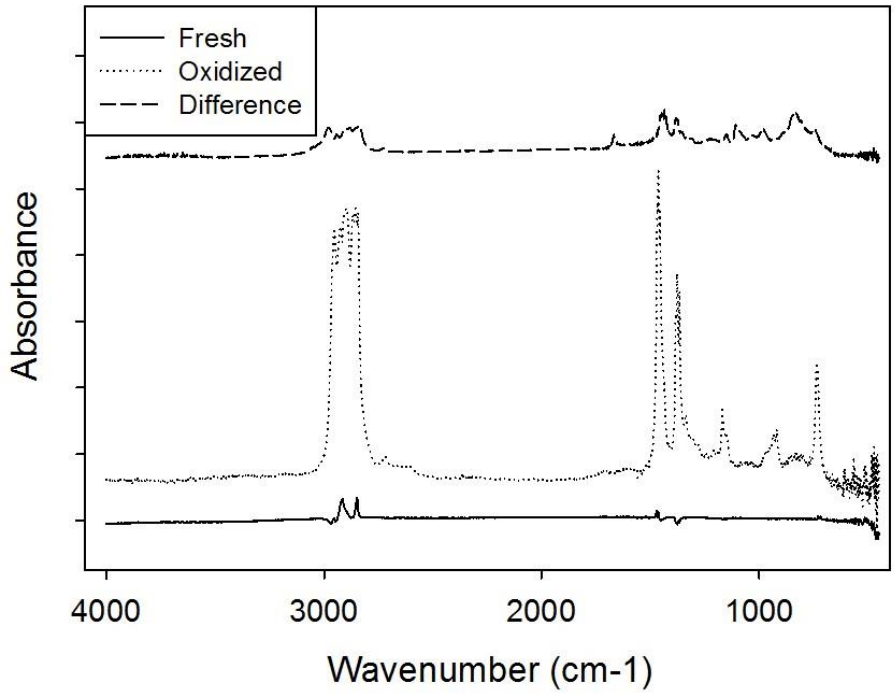

Figure 14: FTIR-HATR spectra for squalane. Major peaks in the difference spectrum are identified and discussed further in the text.

In the squalane difference spectrum for FTIR-HATR (Figure 14), the major peak at 2900 cm^{-1} is for an alkane C-H stretch. Similarly, the peak near 1490 cm^{-1} is representative of a –C-H bend for an alkane. To see the oxidative effects, the peak at 1675 cm^{-1} is important. This peak is for a C=O stretch for a carbonyl. Furthermore, the peaks around 1000 cm^{-1} are for a C-O stretch associated with an alcohol functional group. The introduction of the oxygen molecule indicates that the ozone exposure has caused changes to the squalane structure.

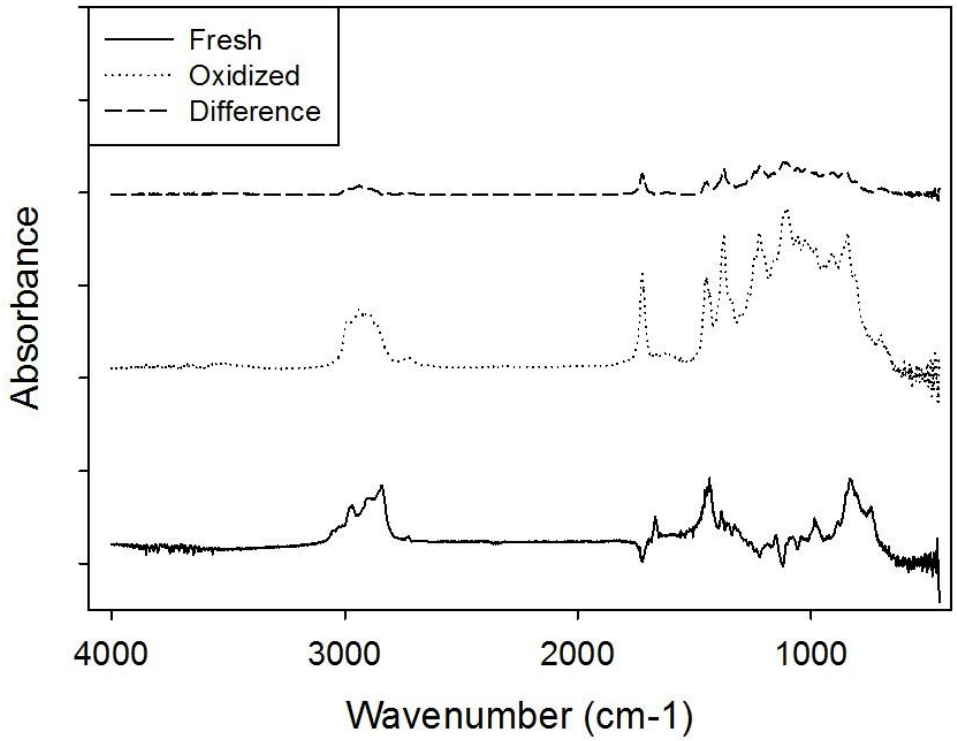

Figure 15: FTIR-HATR spectra for Squalene. Major peaks in the difference spectrum (oxidized-fresh) are identified and discussed further in the text.

Peaks in the FTIR-HATR difference spectrum of squalene (Figure 15) near 3000 cm^{-1} and 1470 cm^{-1} are characteristic of =C-H stretch and C-H bend bonds associated with the organic hydrocarbon. Peaks at 1720 cm^{-1} and between 1320-1000 cm^{-1} illustrate the oxidation effects. The peak at 1720 cm^{-1} is a C=O stretch associated with aldehydes and saturated aliphatics. The group of peaks between 1320-1000 cm^{-1} are associated with a C-O stretch related to alcohols, carboxylic acids, esters, and ethers (Figure 15). Together, the Raman and FTIR-HATR difference spectra depict the effects of oxidation on the sample and confirm that oxidation has occurred.

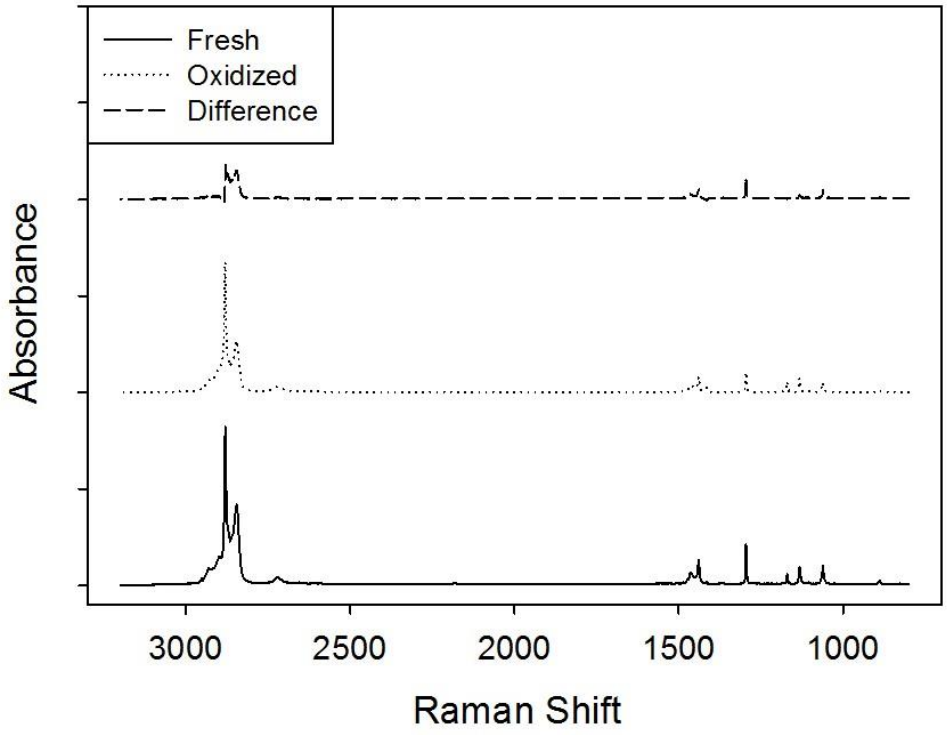

Figure 16: Raman spectra for octacosane, taken at the particle surface. Major peaks in the difference spectrum are identified and discussed further in the text.

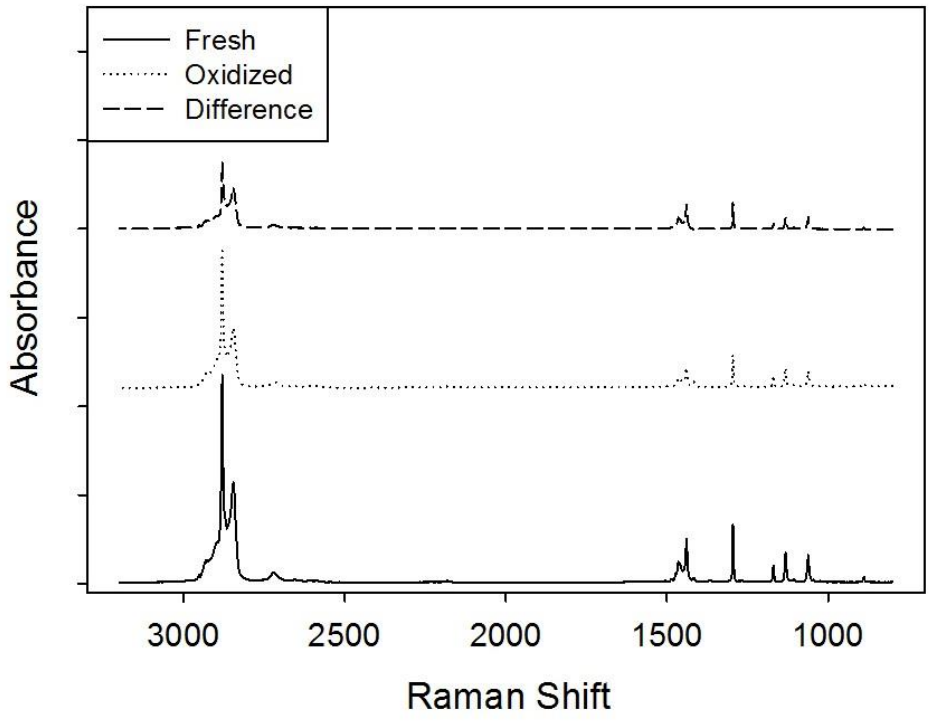

Figure 17: Raman spectra for octacosane bulk. Major peaks in the difference spectrum are identified and discussed further in the text.

As described previously, the solid octacosane samples were characterized in two different ways with the Raman. First, a 50 micron pinhole was used to examine the surface of the material (Figure 16). Next, a 200 micron pinhole was used to study the bulk of the material (Figure 17). The purpose of looking at both the surface and the bulk was to identify whether the oxidation was penetrating the bulk of the sample instead of just altering the surface. In both Figure 16 and 17, the peaks in the difference spectrum in the 2800 cm^{-1} range represent the C-H bond of an alkane and the peak near 1490 cm^{-1} is characteristic of a $–CH_3$ bend for an alkane. To better illustrate the differences

between the surface and the bulk oxidation, the difference between the two is plotted (Figure 18). To ensure a fair comparison, this data was calculated by subtracting the bulk data from the surface data for both the fresh and oxidized data. The resulting set of data was a fresh octacosane difference and an oxidized octacosane difference. From this set of data, a difference spectrum was created by subtracting the fresh data from the oxidized data. The resulting peaks indicate differences between oxidative effects on the surface and bulk of the octacosane samples.

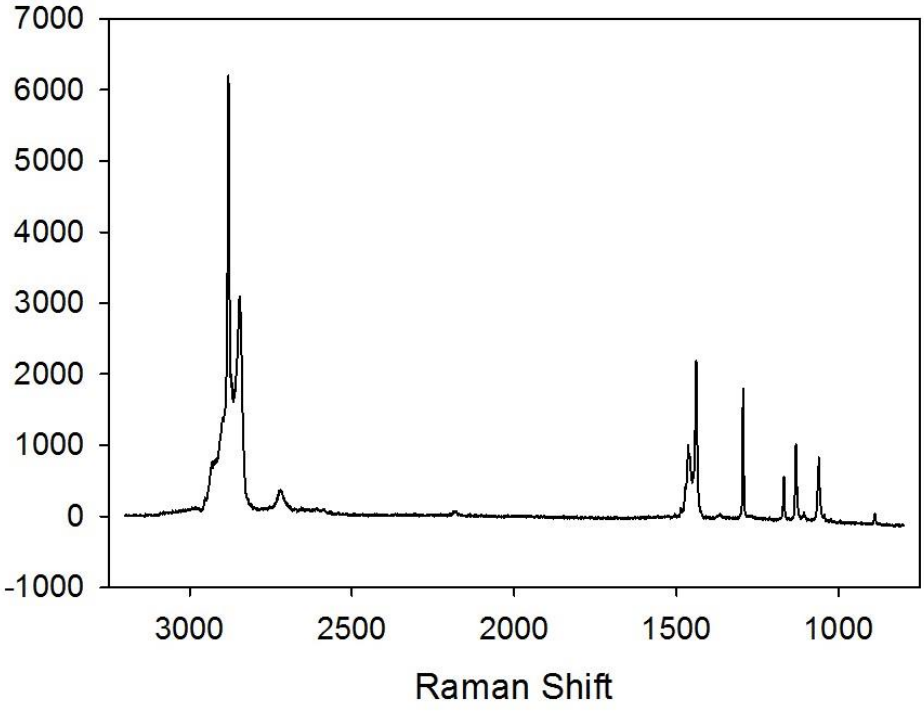

Figure 18: Raman difference spectrum illustrating changes between the surface and bulk oxidation effects.

Since all of the peaks in Figure 18 are positive, it may be concluded that more oxidation occurs on the surface of the octacosane particle than in the bulk. This is what was hypothesized for a solid sample. Internal mixing occurs at a slow pace for solids, so it is expected that the majority of the oxidation occurs at the surface. This indicates that changes are occurring at the particle surface which could be affecting the freezing ability of the IN. For experimental reasons, the same procedure could not be completed for the liquid samples. It is assumed that the high rate of internal mixing in liquids causes the surface and bulk of the sample to display similar characteristics. Figure 18 also helps confirm that oxidation has occurred for the octacosane. Each of the peaks can be identified to ensure oxidative effects for the overall particle. The peak at 2875 cm^{-1} indicates a change in peak intensity for the $–CH_3$ and $–CH_2$- stretches for an alkane group. The peak located at 2850 cm^{-1} is the first indication of oxidative effects. This peak is for a $–CH_3$ attached to an oxygen molecule. Similarly, a peak at 2720 cm^{-1} indicates a CHO bend for an aldehyde. Further evidence is shown by the peaks at 1170 cm^{-1}, 1130 cm^{-1}, and 1100 cm^{-1}, which all represent a C-O-C stretch for esters, ethers, and alcohols. Another change occurs at 1295 cm^{-1} for a C-C bond in an alcohol, ether, ester, carboxylic acid, or anhydride. The final piece of evidence of oxidation for octacosane is the peak located at 1060 cm^{-1} which is for a C-O stretch associated with an alcohol. All of these changes indicating the addition of an oxygen molecule offer proof that exposure to ozone has caused alterations in the make-up of the octacosane molecule.

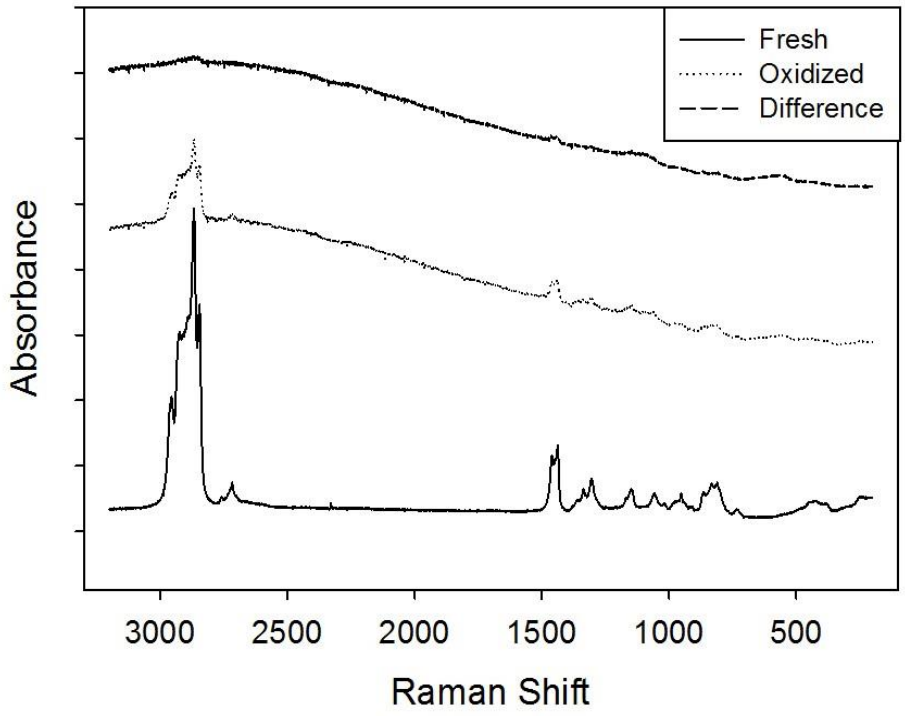

Figure 19: Raman spectra for squalane. Major peaks for the difference spectrum are identified and discussed in the text.

The Raman difference spectra for squalane also displays ample evidence of oxidation (Figure 19). The peaks at 2860 cm^{-1} and 1450 cm^{-1} are a $–CH_3$ stretch or $-CH_2-$ stretch for an alkane. Oxidation is seen in the peak at 1085 cm^{-1}, which indicates a C-O stretch for an alcohol. Finally, the peak at 560 cm^{-1} peak can be interpreted as a C-C=O bend representative of a ketone.

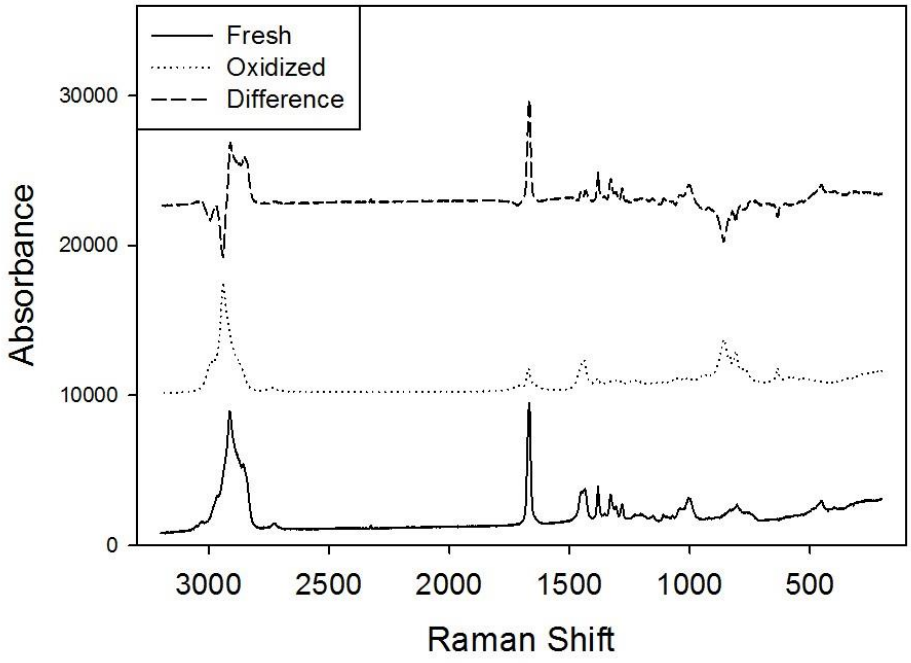

Figure 20: Raman spectra for Squalene. Major peaks in the difference spectrum (oxidized-fresh) are identified and discussed in the text.

A difference spectrum is also calculated for the Raman spectra to characterize the difference between the oxidation spectrum and the spectrum from the fresh sample. Peaks are identified in the difference spectra to assess the functional groups seen. Peaks near 2950 cm^{-1}, 1450 cm^{-1}, and between 850-800 cm^{-1} in the Raman difference spectrum of squalene (Figure 20) all characterize various C-H bonds (stretches, bends, and out of plane bends, respectively) associated with the organic hydrocarbon. Similarly, the peak at 1440 cm^{-1} is for a C=C stretch characteristic of an alkene. The interesting difference to note is the new peak at 630 cm^{-1}. This peak represents a O-C=O bond, characteristic of a

ketone or carboxylic acid. This peak implies oxidation of the squalene by showing the addition of an oxygen bond.

3.5 Role of Oxidation in Ice Nucleation

Similar to previous work with solid samples such as soot and polycyclic aromatic hydrocarbons (Brooks et al., 2014), the octacosane shows a slight improvement in ice nucleation ability with oxidation. Oxidation is known to increase hydrophilicity, which reduces the contact angle between the water droplet and the surface. This may cause an improvement in ice nucleation ability. However, results from this study show this to not always be the case. While the squalene also shows an improvement in IN ability with oxidation, the squalane has the opposite effect. When squalane is oxidized, it becomes a less efficient IN by about 1 degree. This may be due to differences in the effects of oxidation on solids and liquids. As observed in the octacosane spectra, oxidation of solids results in changes to the surface features of the IN. While not observable in this study due to limitations of the Raman instrument, oxidation of liquids generally causes changes in the bulk. Solid samples tend to have a slower rate of internal mixing than that of liquids. Therefore, it is mostly the surface of a solid sample that is altered via oxidation, whereas the liquid samples are more uniform throughout.

Differences between the effects of oxidation on the two liquid hydrocarbons may be explained by the different molecular level interactions with ozone. The two different molecules are going through either fragmentation or functionalization. Fragmentation is the process by which a molecule is broken down, or fragmented, during an interaction. Conversely, functionalization occurs when the initial molecule is added on to and

becomes larger during interaction. These molecular effects have important implications on the effectiveness of an IN.

The changes in viscosity by oxidation add evidence to the idea of fragmentation and functionalization occurring. Oxidation of squalane results in a slight decrease of viscosity, while the same process causes a marked increase in viscosity for squalene. Each liquid sample is undergoing a different molecular interaction with the ozone during oxidation. The squalane is being fragmented and the squalene is being functionalized. Larger molecules correspond to a higher viscosity. This explains why the functionalization that occurs during oxidation of squalene would result in a much more viscous liquid, since the molecules are becoming larger. Counter to this, the fragmentation of squalane during oxidation results in a reduction in viscosity due to molecules becoming smaller.

3.6 Role of Viscosity in Ice Nucleation

To analyze the viscosity change between fresh and oxidized squalane and squalene, a viscometer was used to measure the dynamic viscosity (Figure 7). In addition to measuring viscosity change as a result of oxidation, the viscometer was also used to measure the change in viscosity with temperature. If the viscosity of the sample changed significantly upon cooling, it is possible this could affect the IN ability of the sample. As a sample cools, the molecules within it will begin to move more slowly, so the sample will naturally become more viscous. However, degree to which the viscosity changes is variable for each sample. Olive oil, water, and ethylene glycol were also measured using the viscometer for comparison purposes. Note that the olive oil froze

at -10 °C, the water froze at 0 °C, and the ethylene glycol froze at -30 °C and thus could not be tested for viscosity after this point. Likewise, the viscosity of oxidized squalene became too high to measure with the available technique at temperatures below room temperature (~23.5 °C). The timescale for measuring the movement of squalene through the viscometer was on the order of ~9 hours, resulting in a substance with a high viscosity between that of peanut butter and sour cream (1330.26 poise). Table 4 compares the viscosity of the samples used in this study with substances of known viscosity.

Table 4: Viscosity comparison table including samples measured in this study. The viscosities are reported for approximate room temperature. Samples measured in this study are marked with an asterisk.

Material	Viscosity (Poise)
Water	0.01
Milk	0.03
Oxidized Squalane*	0.07
Fresh Squalene*	0.14
Ethylene Glycol*	0.18
Fresh Squalane*	0.31
Olive Oil*	0.69
SAE 10 Motor Oil	0.85-1.4
SAE 20 Motor Oil	1.4-4.2
SAE 30 Motor Oil	4.2-6.5
SAE 40 Motor Oil	6.5-9.0
Castrol™ Oil	10
Karo™ Syrup	50
Honey	100
Chocolate	250
Ketchup	500
Mustard	700
Sour Cream	1000
Oxidized Squalene*	1330.26
Peanut Butter	2500

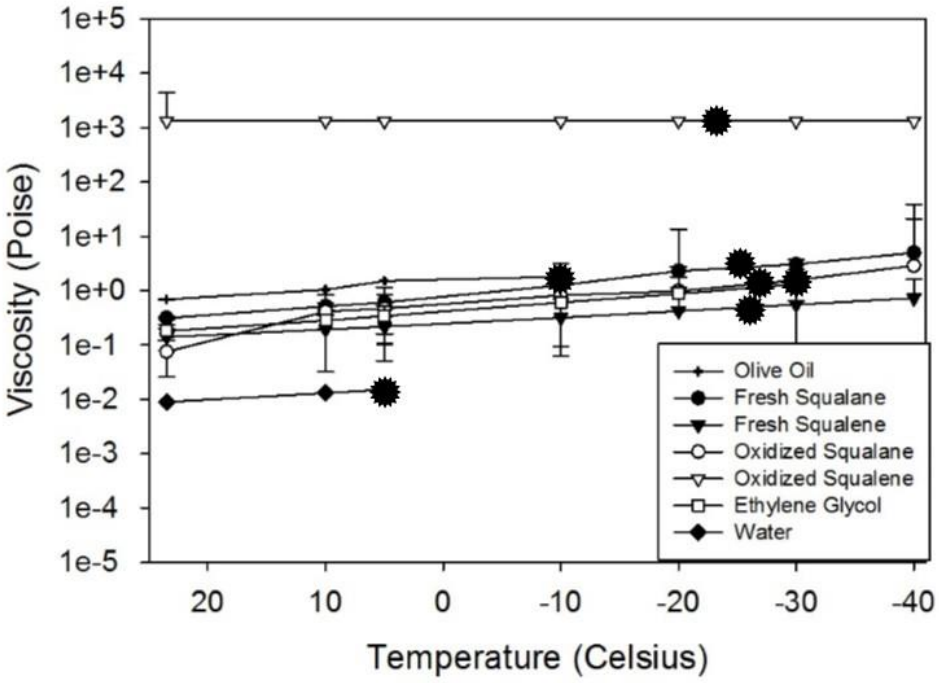

Figure 21: Change in viscosity with decreasing temperature. Stars indicate the point at which contact freezing was initiated during ice microscope experiments.

Observed viscosities as a function of temperature are plotted in Figure 21. For each sample, there is a trend towards higher viscosity as the temperature decreases. Stars are used to indicate the observed mean freezing temperature associated with contact freezing events for the samples tested in this study. All of the samples are more viscous than water, which could provide evidence for the propensity of aerosols with a viscosity higher than that of water to act as ice nuclei. Our results imply that the hydrocarbons acting as INP in this study have viscosity of 0.49 poise or greater at the freezing temperature. One possible interpretation is that particles may be acting as flexible ice nuclei, which is discussed further in the following section. Unfortunately, the results did

not reveal a single “critical” minimum viscosity required for all samples to act as an INP.

Overall, the squalane, which becomes less viscous when oxidized, also shows a decrease in IN ability with aging. This is opposite of the squalene, which becomes more viscous when oxidized, and improves in IN ability with aging. The oxidation of squalane also has an opposite effect compared to oxidation of octacosane. Both squalene and octacosane become more efficient IN when aged. This is represented again in Figure 22, alongside previous work on soot and polycyclic aromatic hydrocarbons (Fornea et al., 2009; Brooks et al., 2014).

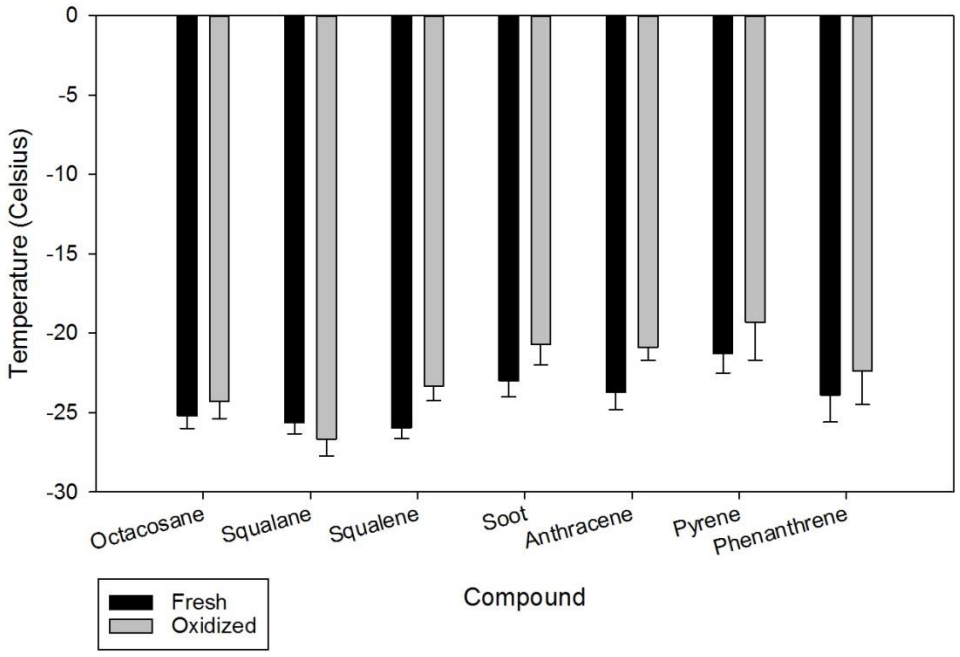

Figure 22: Contact freezing temperatures for the organic hydrocarbons tested in this study and previous work with soot and polycyclic aromatic hydrocarbons (Brooks et al., 2014).

Figure 22 depicts the similar freezing temperatures among all of the organic hydrocarbons studied (~-25 °C). The minor differences are likely due to the slight differences in structure for each compound.

3.7 Simplified Soccer Ball Model

Next, the simplified Soccer Ball Model was used to compare model to theory and to derive values of the wetting parameters and contact angles of each INP in this study. Some assumptions have been made for this application of classical nucleation theory. It is assumed the surface sites of the entire surface area of the IN interact with the water droplet. Second, the liquid IN are assumed to be spherical in order to calculate the diameter. This is a limiting factor since the liquid IN actually pooled out around the spherical water droplet instead of forming a sphere. Using these assumptions, we can estimate the fraction of droplets that are frozen at a given temperature and evaluate differences based on composition and aging state of the IN. These calculations are commonly used to assess IN (Brooks et al., 2014; Zobrist et al., 2007; Fornea et al., 2009; Niedermeier et al., 2014).

To determine the empirical probability for one compound, all data points collected during all experiments runs were collected into a single data set to determine the empirical probability of freezing. This probability is linked as a function of temperature to the theoretical probability by:

$$P(Temp) = \frac{N_f}{N_0} = 1 - \exp(-\frac{dt}{dT}\int_{T_0}^{T} j_{het'} dT)$$

where N_0 is the total number of water droplets, N_f is the number of water droplets that have frozen, T is temperature, t is time, and $j_{het,}$ represents the nucleation rate coefficients (Brooks et al., 2014; Shaw et al., 2005).

Equations 1-5 and parameters from Zobrist et al. (2007) were used to determine the theoretical probability of freezing, P_{fr}, for each sample. Wetting parameter was derived by determining the best fit of the theoretical probability to the empirical probability defined based on the data. The contact angle could then be calculated using equation from Zobrist et al. (2007). Figure 23 illustrates the combined empirical probability of freezing with the theoretical curve generated for each fresh and oxidized sample. The theoretical curve was adjusted to align with the empirical curve at approximately the 50% probability level. This was accomplished by altering the mean contact angle, μ_θ, to match a fraction frozen of 0.5 on the empirical curve. Adjusting the mean contact angle transforms the graph by sliding the curve along the x axis. Adjusting the standard deviation in contact angle, σ_θ, allows for control of the tilt in the probability function. The value of σ_θ was adjusted to align with the majority of the empirical data points.

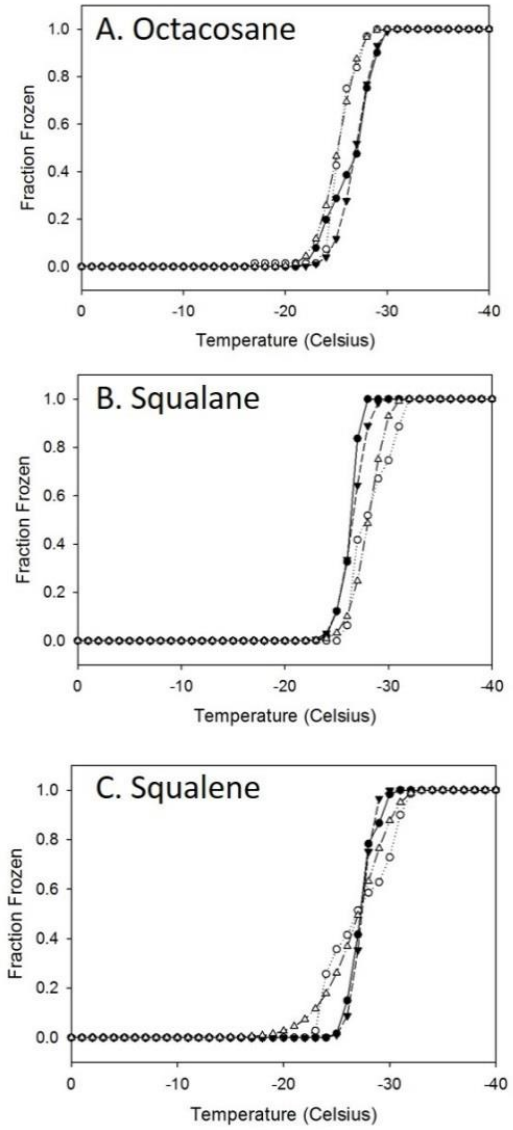

Figure 23: Fraction frozen for 275 micron octacosane and ~781 micron squalane and squalene are shown in part A, B, and C, respectively. The empirical probabilities of freezing fresh and oxidized IN are shown as solid and open circles, respectively, in each panel. The theoretical fraction frozen best fit to the data for fresh and oxidized samples are depicted as solid and open triangles, respectively.

As illustrated by Figure 23, the effect of oxidation varies with INP composition. The octacosane induces freezing at warmer temperatures after oxidation. This aligns

with previous work using solid samples such as soot and polycyclic aromatic hydrocarbons (Brooks et al., 2014). However, the oxidized squalene shows a tendency to transition from more to less effective IN ability compared to fresh squalene as the temperature decreases. According to this theory (which doesn't take viscosity into account), IN efficiency is linked to the hydrophilicity of the particle. A more hydrophilic particle will have a lower contact angle and correspond to a smaller wetting parameter. Table 5 indicates this trend with lower f values aligning with lower contact angles. The simplified Soccer Ball model does not specifically take viscosity into account. Further studies are needed to determine the combined influences of viscosity and oxidation on the kinetics of molecular rearrangement prior to nucleation as well as the nucleation rates.

Table 5: Derived values of mean contact angle, θ, with the standard deviation in contact angle, and the wetting parameter, f, for all IN compositions in this study.

IN Composition	Size (μm)	Contact Angle, θ (degrees)	Wetting Parameter, f
Octacosane, fresh	275	85.94 ± 5.16	0.81
Octacosane. Oxidized	275	80.21 ± 5.16	0.42
Squalane, fresh	~781	85.94 ± 4.30	0.81
Squalane, oxidized	~781	91.67 ± 5.73	0.98
Squalene, fresh	~781	88.81 ± 3.44	0.07
Squalene, oxidized	~781	88.81 ± 10.60	0.07

4. ATMOSPHERIC IMPLICATIONS AND CONCLUSIONS

The role of organic hydrocarbons in heterogeneous freezing processes is not well constrained. In this study, we report on contact freezing experiments for the fresh and oxidized organic hydrocarbons octacosane, squalane, and squalene. As aerosols travel through the atmosphere, they are exposed to different aging processes that alter their characteristics and IN ability. This was represented through oxidative aging of the samples in the study. The average freezing temperature of these compounds in their fresh forms was -25.6°C. Oxidation improved IN ability for the solid sample, octacosane, by an average of 1 °C which is in line with previous work with soot and PAHs, although oxidation caused a larger improvement of 2-3 °C on average for these compounds. Varying molecular effects on liquid samples due to oxidation resulted in different IN ability.

From the preceding results and previous work (Fornea et al., 2009; Brooks et al., 2014), we conclude that organics act as moderately effective ice nuclei with only slight variations in efficiency due to surface structure. Soot, PAHs, and straight chain hydrocarbons have all shown to cause heterogeneous nucleation near -25°C even though they each have vastly different structures. Despite this similarity, there are minor differences in freezing temperature that are likely due to the surface characteristics of these substances.

The main focus of this study was to assess the ability of organic hydrocarbons to act as ice nuclei in the contact freezing mode and to evaluate how oxidative aging affects

this ability. FTIR-HATR spectroscopy and Raman microspectroscopy both show evidence of oxidation via the addition of oxygen bonding after oxidation. This is illustrated in the difference spectra calculated for each sample. The Raman spectra also indicated differences in surface and bulk oxidation effects for the solid sample, octacosane. The surface of the solid sample indicated greater oxidative effects than that of the bulk. This is due to the slow internal mixing characteristic of a solid particle. This result suggests that the greatest change in the particle's features occurs at the surface, where it can highly influence the contact freezing ability of the IN.

Oxidation affected each sample studied in a different way. As previous group work suggests (Fornea et al, 2009; Brooks et al., 2014), the solid sample, octacosane, showed an improvement in IN ability with oxidation by 1-2 degrees. Changes brought about by exposure to ozone cause the particles to be more wettable, as indicated by a decrease in the wetting parameter. This corresponds to a particle that has become more hydrophilic. As a particle becomes more hydrophilic, the contact angle decreases. A decrease in the contact angle yields a higher propensity for the water droplet to freeze at warmer temperatures. This behavior did not necessarily translate to the same result for the liquid samples though. The effects of oxidation on the liquid samples is discussed in more detail below.

The most notable find in this study is the ability of liquids to act as IN. Experiments were performed to ensure the liquid samples were not mixing with the water droplet or freezing prior to acting as an IN. These findings suggest that aerosol phase is not necessarily a determinant in the role a particle plays in ice nucleation.

During oxidation of liquids, a noticeable change in viscosity occurred in the squalene sample in particular. This observation combined with knowledge of glasses, gels, and amorphous solids acting as IN led to the idea of viscosity affecting IN ability. All liquid samples were tested for changes in viscosity caused by oxidation as well as changes associated with decreasing temperature throughout the experimental runs. Measurements taken with a viscometer indicated an increase in viscosity with temperature for all samples. However, oxidation impacted the viscosity of the samples in various ways. Since viscosity it known to increase as the temperature decreases, it was originally hypothesized that some critical viscosity needed to be reached for nucleation to occur. However, Figure 21 does not indicate any major dependence on the degree of viscosity between substances. Freezing occurs at various, albeit similar, temperatures in the liquids tested, despite their wide range in viscosities. Conversely, there does seem to be a slight dependence on viscosity and ice nucleation ability between a fresh and oxidized sample. For example, the squalane shows a marked decrease in IN ability of about 1°C with oxidation. As discussed previously, this is related to the molecular processes occurring during oxidation. As the squalane is fragmented, it becomes less viscous since the molecules become smaller, and thus it becomes less effective as an IN. On the other hand, squalene shows an increase in IN ability with oxidation by about 2°C. Again, this can be attributed to the molecular processes. When undergoing oxidative aging, the squalene is functionalized, becoming a larger molecule and thus more viscous. This more viscous product acts as a more effective IN. This again illustrates that there may be a slight dependence on surface structure in ice nucleation ability. Although, these

findings contribute a great deal to the role of liquids as IN, further study is needed on the implications of viscosity changes on the ice nucleating ability of liquids.

In order for these liquids to act as ice nuclei, it is believed that they are behaving as flexible IN. This concept has been discussed in Ochshan and Cantrell (2006), and more recently in Zielke et al. (2015). This theory involves the movement of molecules at the surface of both the IN and the water droplet. Traditional theory calls for a crystalline structure to act as a template for the water molecules to form the necessary structure for ice. With a flexible IN, the molecules in the aerosol and the molecules in the water droplet are both working in conjunction to form a crystalline structure. In this way, not only are the water molecules adapting to the surface of the IN, but the IN is also adapting to the surface of the ice. By the molecules in both the droplet and the IN working together, the energy barrier is lowered—making it possible for the flexible IN to cause the droplet to freeze heterogeneously. More insight can be gained by conducting additional experiments with flexible ice nuclei. A higher level of understanding could also be accomplished through more extensive modeling of flexible ice nuclei to gain a better understanding of what is occurring on the molecular level.

Overall, oxidative aging tends to improve the ability of solid aerosols to act as IN, but the effect on liquids differs depending on what molecular processes occur. Due to the effects of fragmentation and functionalization, viscosity was decreased and increased, respectively. This resulted in the oxidized squalane becoming less viscous and the oxidized squalene becoming more viscous than their fresh counterparts. Effects on

the IN ability of these compounds corresponds slightly to the viscosity. An increase in viscosity led to an increase in IN ability and vice versa.

The combined effects of fragmentation and functionalization with their implications on viscosity are shown to have predictable impacts on the behavior of an ice nuclei. The finding of liquid aerosols acting as IN could have tremendous atmospheric impacts. This opens up an entirely new set of aerosols to be studied as ice nuclei and could lead to improvements in models. Future work needs to be performed to improve characterization of liquids as ice nuclei and further investigate the role of viscosity in IN ability.

REFERENCES

Avzianova, E. and Brooks, S.D., 2013. Raman spectroscopy of glyoxal oligomers in aqueous solutions. *Spectrochimica Acta Part A: Molecular and Biomolecular Spectroscopy*, *101*, pp.40-48.

Avzianova, E. and Brooks, S.D., 2014. Analysis of nickel (II) in particulate matter by Raman microspectroscopy. *Journal of Aerosol Science*, *67*, pp.207-214.

Baustian, K.J., Wise, M.E., Jensen, E.J., Schill, G.P., Freedman, M.A. and Tolbert, M.A., 2013. State transformations and ice nucleation in amorphous (semi-) solid organic aerosol. *Atmospheric Chemistry & Physics*, *13*(11), pp5615-5628.

Bogdan, A., Molina, M.J., Tenhu, H. and Loerting, T., 2014. Multiple glass transitions and freezing events of aqueous citric acid. *The Journal of Physical Chemistry A*, *119*(19), pp.4515-4523.

Brooks, S.D., Suter, K. and Olivarez, L., 2014. Effects of chemical aging on the ice nucleation activity of soot and polycyclic aromatic hydrocarbon aerosols. *The Journal of Physical Chemistry A*, *118*(43), pp.10036-10047.

Cappa, C.D. and Wilson, K.R., 2011. Evolution of organic aerosol mass spectra upon heating: implications for OA phase and partitioning behavior.*Atmospheric Chemistry and Physics*, *11*(5), pp.1895-1911.

Debenedetti, P.G. and Stillinger, F.H., 2001. Supercooled liquids and the glass transition. *Nature*, *410*(6825), pp.259-267.

Deng, C., Brooks, S.D., Vidaurre, G. and Thornton, D.C., 2014. Using Raman microspectroscopy to determine chemical composition and mixing state of airborne marine aerosols over the Pacific Ocean. *Aerosol Science and Technology*, *48*(2), pp.193-206.

Dette, H.P. and Koop, T., 2014. Glass formation processes in mixed inorganic/organic aerosol particles. *The Journal of Physical Chemistry A*,*119*(19), pp.4552-4561.

Fornea, A.P., Brooks, S.D., Dooley, J.B. and Saha, A., 2009. Heterogeneous freezing of ice on atmospheric aerosols containing ash, soot, and soil. *Journal of Geophysical Research: Atmospheres*, *114*(D13); pp.D13201-1—D13201-12.

Hiranuma, N., Möhler, O., Yamashita, K., Tajiri, T., Saito, A., Kiselev, A., Hoffmann, N., Hoose, C., Jantsch, E., Koop, T. and Murakami, M., 2015. Ice nucleation by cellulose and its potential contribution to ice formation in clouds. *Nature Geoscience*, *8*(4), pp.273-277.

Hoose, C. and Möhler, O., 2012. Heterogeneous ice nucleation on atmospheric aerosols: a review of results from laboratory experiments.*Atmos. Chem. Phys*, *12*(20), pp.9817-9854.

Ignatius, K., Kristensen, T.B., Järvinen, E., Nichman, L., Fuchs, C., Gordon, H., Herenz, P., Hoyle, C.R., Duplissy, J., Garimella, S. and Dias, A., 2015. Heterogeneous ice nucleation of viscous secondary organic aerosol produced from ozonolysis of α-pinene. *Atmospheric Chemistry & Physics Discussions*, *15*(24), pp. 6495-6509.

Knopf, D.A., Alpert, P.A., Wang, B. and Aller, J.Y., 2011. Stimulation of ice nucleation by marine diatoms. *Nature Geoscience*, *4*(2), pp.88-90.

Knopf, D.A. and Koop, T., 2006. Heterogeneous nucleation of ice on surrogates of mineral dust. *Journal of Geophysical Research: Atmospheres*,*111*(D12), pp. D12201-1—D12201-10.

Koop, T., Bookhold, J., Shiraiwa, M. and Pöschl, U., 2011. Glass transition and phase state of organic compounds: dependency on molecular properties and implications for secondary organic aerosols in the atmosphere. *Physical Chemistry Chemical Physics*, *13*(43), pp.19238-19255.

Lupi, L. and Molinero, V., 2014. Does hydrophilicity of carbon particles improve their ice nucleation ability?. *The Journal of Physical Chemistry A*,*118*(35), pp.7330-7337.

Murray, B.J., 2008. Inhibition of ice crystallisation in highly viscous aqueous organic acid droplets. *Atmospheric Chemistry and Physics*, *8*(17), pp.5423-5433.

Murray, B.J. and Bertram, A.K., 2008. Inhibition of solute crystallisation in aqueous H+–NH 4+–SO 4 2−–H2O droplets. *Physical Chemistry Chemical Physics*, *10*(22), pp.3287-3301.

Niedermeier, D., Shaw, R.A., Hartmann, S., Wex, H., Clauss, T., Voigtländer, J. and Stratmann, F., 2011. Heterogeneous ice nucleation: exploring the transition from stochastic to singular freezing behavior. *Atmospheric Chemistry and Physics*, *11*(16), pp.8767-8775.

Niedermeier, D., Ervens, B., Clauss, T., Voigtländer, J., Wex, H., Hartmann, S. and Stratmann, F., 2014. A computationally efficient description of heterogeneous

freezing: A simplified version of the Soccer ball model.*Geophysical Research Letters*, *41*(2), pp.736-741.

Perraud, V., Bruns, E.A., Ezell, M.J., Johnson, S.N., Yu, Y., Alexander, M.L., Zelenyuk, A., Imre, D., Chang, W.L., Dabdub, D. and Pankow, J.F., 2012. Nonequilibrium atmospheric secondary organic aerosol formation and growth. *Proceedings of the National Academy of Sciences*, *109*(8), pp.2836-2841.

Perraudin, E., Budzinski, H. and Villenave, E., 2007. Identification and quantification of ozonation products of anthracene and phenanthrene adsorbed on silica particles. *Atmospheric Environment*, *41*(28), pp.6005-6017.

Perraudin, E., Budzinski, H. and Villenave, E., 2007. Kinetic study of the reactions of ozone with polycyclic aromatic hydrocarbons adsorbed on atmospheric model particles. *Journal of Atmospheric Chemistry*, *56*(1), pp.57-82.

Pöschl, U., 2011. Gas–particle interactions of tropospheric aerosols: Kinetic and thermodynamic perspectives of multiphase chemical reactions, amorphous organic substances, and the activation of cloud condensation nuclei. *Atmospheric Research*, *101*(3), pp.562-573.

Schill, G.P. and Tolbert, M.A., 2013. Heterogeneous ice nucleation on phase-separated organic-sulfate particles: effect of liquid vs. glassy coatings.*Atmospheric Chemistry and Physics*, *13*(9), pp.4681-4695.

Schill, G.P., De Haan, D.O. and Tolbert, M.A., 2014. Heterogeneous ice nucleation on simulated secondary organic aerosol. *Environmental science & technology*, *48*(3), pp.1675-1682.

Seinfeld, J.H. and Pandis, S.N., 2016. *Atmospheric chemistry and physics: from air pollution to climate change*. John Wiley & Sons, Hoboken, New Jersey.

Shaw, R.A., Durant, A.J. and Mi, Y., 2005. Heterogeneous surface crystallization observed in undercooled water. *The Journal of Physical Chemistry B*, *109*(20), pp.9865-9868.

Shiraiwa, M., Ammann, M., Koop, T. and Pöschl, U., 2011. Gas uptake and chemical aging of semisolid organic aerosol particles. *Proceedings of the National Academy of Sciences*, *108*(27), pp.11003-11008.

Virtanen, A., Joutsensaari, J., Koop, T., Kannosto, J., Yli-Pirilä, P., Leskinen, J., Mäkelä, J.M., Holopainen, J.K., Pöschl, U., Kulmala, M. and Worsnop, D.R., 2010. An amorphous solid state of biogenic secondary organic aerosol particles. *Nature*, *467*(7317), pp.824-827.

Wagner, R., Möhler, O., Saathoff, H., Schnaiter, M., Skrotzki, J., Leisner, T., Wilson, T.W., Malkin, T.L. and Murray, B.J., 2012. Ice cloud processing of ultra-viscous/glassy aerosol particles leads to enhanced ice nucleation ability. *Atmos. Chem. Phys*, *12*(18), pp.8589-8610.

Welti, A., Kanji, Z.A., Lüönd, F., Stetzer, O. and Lohmann, U., 2014. Exploring the mechanisms of ice nucleation on kaolinite: from deposition nucleation to condensation freezing. *Journal of the Atmospheric Sciences*,*71*(1), pp.16-36.

Wilson, T.W., Murray, B.J., Wagner, R., Möhler, O., Saathoff, H., Schnaiter, M., Skrotzki, J., Price, H.C., Malkin, T.L., Dobbie, S. and Al-Jumur, S.M.R.K., 2012. Glassy aerosols with a range of compositions nucleate ice heterogeneously at cirrus temperatures. *Atmospheric Chemistry and Physics*, *12*(18), pp.8611-8632.

Zielke, S.A., Bertram, A.K. and Patey, G.N., 2015. Simulations of ice nucleation by kaolinite (001) with rigid and flexible surfaces. *The Journal of Physical Chemistry B*, *120*(8), pp.1726-1734.

Zobrist, B., Koop, T., Luo, B.P., Marcolli, C. and Peter, T., 2007. Heterogeneous ice nucleation rate coefficient of water droplets coated by a nonadecanol monolayer. *The Journal of Physical Chemistry C*, *111*(5), pp.2149-2155.